



Non-noble metal catalysts for hydrogenation: A facile method for preparing Co nanoparticles covered with thin layered carbon



Lichen Liu, Patricia Concepción, Avelino Corma^{*}

Instituto de Tecnología Química, Universidad Politécnica de Valencia-Consejo Superior de Investigaciones Científicas (UPV-CSIC), Av. de los Naranjos s/n, 46022 Valencia, Spain

ARTICLE INFO

Article history:

Received 17 December 2015

Revised 29 March 2016

Accepted 9 April 2016

Keywords:

Co nanoparticles

Layered carbon

Chemoselective hydrogenation

Nitroarenes

ABSTRACT

Metallic cobalt nanoparticles with surface CoO_x patches covered by thin layered carbon (named Co@C) have been directly synthesized by thermal decomposition of Co-EDTA complex. Raman spectra and HRTEM images suggest that discontinuities can be found in the disordered layered carbon. XPS shows that the CoO_x patches in the Co@C nanoparticles can be reduced to metallic Co by H_2 under reaction conditions (7 bar at 120 °C), and H_2 - D_2 exchange experiments show that the reduced metallic Co nanoparticles covered by carbon layers can dissociate H_2 . The Co@C nanoparticles show excellent activity and selectivity during chemoselective hydrogenation of nitroarenes for a wide scope of substrates under mild reaction conditions. Based on the results from DRIFTS adsorption experiments, we propose that metallic Co in the Co@C nanoparticles is the active phase. The role of the carbon layers is to protect the Co from overoxidation by air, leading to the chemoselective hydrogenation of nitroarenes.

© 2016 Elsevier Inc. All rights reserved.

1. Introduction

The chemoselective hydrogenation of nitroarenes is an important hydrogenation reaction for production of fine and bulk chemicals, with wide industrial and pharmaceutical applications [1]. Noble metals such as Au, Pt, Ru, Pd, and Ir have been proved to be active components for hydrogenation of nitroarenes [2,3]. By controlling the metal-support interaction and particle size, the chemoselective hydrogenation of nitroarenes can be carried out with high chemoselectivity [4,5]. However, considering the high price and limited availability of noble metals, it is of interests to develop non-noble metal catalysts for chemoselective hydrogenation reactions.

In the last years, non-noble metal catalysts have attracted much attention due to their comparable properties with those of noble metal catalysts in photocatalysis, in electrocatalysis, and in homogeneous and heterogeneous catalysis [6–9]. Recently, the application of CoO_x @N-doped carbon and Fe_2O_3 @N-doped carbon materials for chemoselective hydrogenation of nitroarenes has been reported [10,11]. In this work, the catalysts work under high-pressure conditions (50 bar of H_2), and the authors claim that metal oxide nanoparticles covered by carbon layers were the active species for the chemoselective hydrogenation and hydrogenation-transfer reaction. In a recent paper, Wang et al. observed the in situ

transformation of CoO_x to metallic Co during the selective hydrogenation of nitroarenes under 30 bar of H_2 , although the catalyst was a mixture of CoO_x and metallic Co [12]. As substitutes for noble metal catalysts, the non-noble metal catalysts should work under conditions similar to those for Pt (3–6 bar of H_2) and Au (9–15 bar of H_2) catalysts. However, the reported catalysts are working under much higher H_2 pressure than noble metal catalysts.

From the above reports, it is still not clear whether metallic Co or CoO_x is the active phase for the selective hydrogenation reaction. Moreover, if one considers that in situ dynamic transformation of metal species can occur under reaction conditions, the real active species in the hydrogenation reaction may not be any of the starting materials. Furthermore, the role of the layered carbon materials in the catalytic mechanism during this catalytic hydrogenation has not been clarified. In some works, the carbon layers can protect metal NPs. For example, Ding et al. prepared supported Ni NPs embedded in carbon nitride layers for hydrogenation of nitrobenzene under strong acid conditions [13]. The carbon layers may also block the access of substrates to the metal NPs. In some previous works [10–12], it was proposed that the hydrogenation reactions occur on the surface of carbon layers. However, considering the impermeability of graphene, H_2 cannot diffuse directly through perfect graphene layers, making it even more difficult to unveil the role of carbon layers in hydrogenation reactions [14,15].

In the first part of this work, by following the thermal decomposition of a Co-EDTA complex, we prepare monodispersed

^{*} Corresponding author.

E-mail address: acorma@itq.upv.es (A. Corma).

Co nanoparticles with a thin carbon shell (Co@C). Compared with conventional method for monodispersed Co nanoparticles, organic ligands are not required here to stabilize the Co nanoparticles. The resultant material can catalyze the chemoselective hydrogenation of nitroarenes under mild reaction conditions similar to Au catalysts (7–10 bars of H_2) with high activity and selectivity (>93%). In the second part of this work, with the help of in situ spectroscopic characterizations, we will show that the selective adsorption of reactants occurs on the surface of cobalt nanoparticles. Metallic Co, instead of CoO_x , is the active phase for the hydrogenation reaction, and the role of the carbon layers is to protect the metallic Co NPs from overoxidation.

2. Experiments

2.1. Preparation of Co@C NPs

The Co@C NPs were prepared through the reduction of Co-EDTA complex by H_2 . The Co-EDTA complex was prepared through a hydrothermal process. First, 6.98 g $Co(NO_3)_2$, 4.47 g Na_2EDTA , and 0.96 g NaOH were dissolved in 20 mL H_2O . Then, 10 mL methanol was added to the mixed aqueous solution temperature under stirring at room temperature. After the formation of a homogeneous solution, 23 mL of the purple solution was transferred into a 35 mL stainless steel autoclave, followed by static hydrothermal processing at 200 °C for 24 h. After cooling to room temperature, the generated precipitates were filtered and washed with deionized water and acetone several times, followed by drying at 100 °C in air for 16 h. The obtained complex was denoted as Co-EDTA. Then Co@C NPs were prepared by reduction of Co-EDTA in H_2 (50 mL/min) at 450 °C for 2 h with a ramp rate of 10 °C/min from room temperature to 450 °C. After the H_2 reduction process at 450 °C, the sample was cooled down to room temperature in H_2 atmosphere. Then the black solid product was stored in a glass vial in ambient environment. The ICP analysis shows that the amount of cobalt in the Co@C NPs is ≥ 95 wt.%. The Co@C–250Air and Co@C–450Air were prepared through the calcination of a Co@C sample in air (50 mL/min) at 250 and 450 °C for 2 h with a ramp rate of 5 °C/min.

2.2. Catalytic studies

The chemoselective hydrogenation of nitroarenes was performed in batch reactors. The reactant, internal standard (dodecane), solvent (toluene or THF), and powder catalyst, as well as a magnetic bar, were added into the batch reactor. After the reactor was sealed, air was purged by flushing two times with 10 bar of hydrogen. Then the autoclave was pressurized with H_2 to the corresponding pressure. The stirring speed was kept at 800 rpm and the size of the catalyst powder was below 0.02 mm to avoid either external or internal diffusion limitation. Finally, the batch reactor was heated to the target temperature. For the kinetic studies, 50 μ L of the mixture was taken out for GC analysis at different reaction times. For the scope studies, 100 μ L of the mixture was taken out for GC analysis. The products were also analyzed by GC–MS.

2.3. Characterization techniques

Samples for electron microscopy studies were prepared by dropping the suspension of Co@C NPs using CH_2Cl_2 as the solvent directly onto holey-carbon-coated nickel grids. All the measurements were performed in a JEOL 2100F microscope operating at 200 kV both in transmission (TEM) and scanning-transmission modes (STEM). STEM images were obtained using a high-angle

annular dark-field detector (HAADF), which allows Z-contrast imaging.

Field-emission scanning electron microscopy (FESEM) measurement was performed with a ZEISS Ultra 55 FESEM. The solid powder sample was adsorbed on conductive carbon tape.

X-ray photoelectron spectra of the catalysts were recorded with a SPECS spectrometer equipped with a Phoibos 150MCD-9 multi-channel analyzer using nonmonochromatic $MgK\alpha$ (1253.6 eV) irradiation. Spectra were recorded using an analyzer pass energy of 30 eV and an X-ray power of 100 W and under an operating pressure of 10^{-9} mbar. The fresh Co@C NPs sample was reduced by H_2 (7 bar) at 120 °C for 60 min in a high-pressure catalytic cell connected, under ultrahigh vacuum, to the XPS analysis chamber. Peak intensities were calculated after nonlinear Shirley-type background subtraction and corrected by the transmission function of the spectrometer. During data processing of the XPS spectra, binding energy (BE) values were referenced to the C1s peak (284.5 eV). CasaXPS software was used for spectra treatment [16].

Raman spectra were recorded at ambient temperature with a 785 nm HPNIR excitation laser on a Renishaw Raman spectrometer (“Reflex”) equipped with an Olympus microscope and a CCD detector. The laser power on the sample was 15 mW and a total of 20 acquisitions were taken for each spectrum.

Hydrogen/deuterium (H/D) exchange experiments were carried out in a flow reactor at 25 and 80 °C. The feed gas consisted of 4 mL/min H_2 , 4 mL/min D_2 , and 18 mL/min argon, and the total weight of catalyst was 180 mg. Reaction products (H_2 , HD, and D_2) were analyzed with a mass spectrometer (Omnistar, Balzers). The Co@C sample was reduced in situ at 450 °C for 2 h with a ramp rate of 10 °C/min from room temperature to 450 °C. Then the temperature was decreased to 25 °C and, once stabilized, the H_2 feed was changed to the reactant gas composition. The temperature was increased to 80 °C and maintained for 1 h.

DRIFT spectra were recorded at room temperature with a Nexus 8700 FTIR spectrometer using a DTGS detector at 4 cm^{-1} resolution. Prior to the adsorption experiments, the ex situ reduced samples were reduced in situ at 120 °C under H_2 for 2 h. After activation, the sample was evacuated at 10^{-2} mbar and nitrobenzene and/or styrene was adsorbed until sample saturation, followed by evacuation (10^{-2} mbar) in order to remove physisorbed species. A commercial DRIFT cell (SPECAC) was used. Spectra were acquired in Kubelka–Munk units.

Powder X-ray diffraction (XRD) was performed in a HTPhilips X'Pert MPD diffractometer equipped with a PW3050 goniometer using $CuK\alpha$ radiation and a multisampling handler.

3. Results and discussions

3.1. Catalyst preparation and characterization

The Co@C NPs were prepared by thermal decomposition of Co-EDTA complex under H_2 at 450 °C. The morphological characterization of Co-EDTA complex can be found in the Supporting Information (see Fig. S1). The morphology of Co@C NPs was characterized by FESEM and TEM. As shown in Fig. S2 and Fig. 1a, the Co@C material is formed by monodisperse metal NPs ranging from ca. 20 to ca. 150 nm. Those Co NPs are covered by carbon layers with thickness ranging from ca. 1 to ca. 10 nm (Fig. 1b). From the HRTEM images (Fig. 1c and d), the lattice fringe of metallic Co can be seen [17]. A further look to the surface structures of the Co NPs makes it possible to observe the crystal lattice fringes of Co_3O_4 , as shown in Fig. S3 [18]. Therefore, one can assume, as a first approximation, that the Co NP can be formed by a core-shell structure with metal Co at the core and CoO_x as the shell. In order to know the chemical composition of the Co@C sample, STEM-HAADF elemental

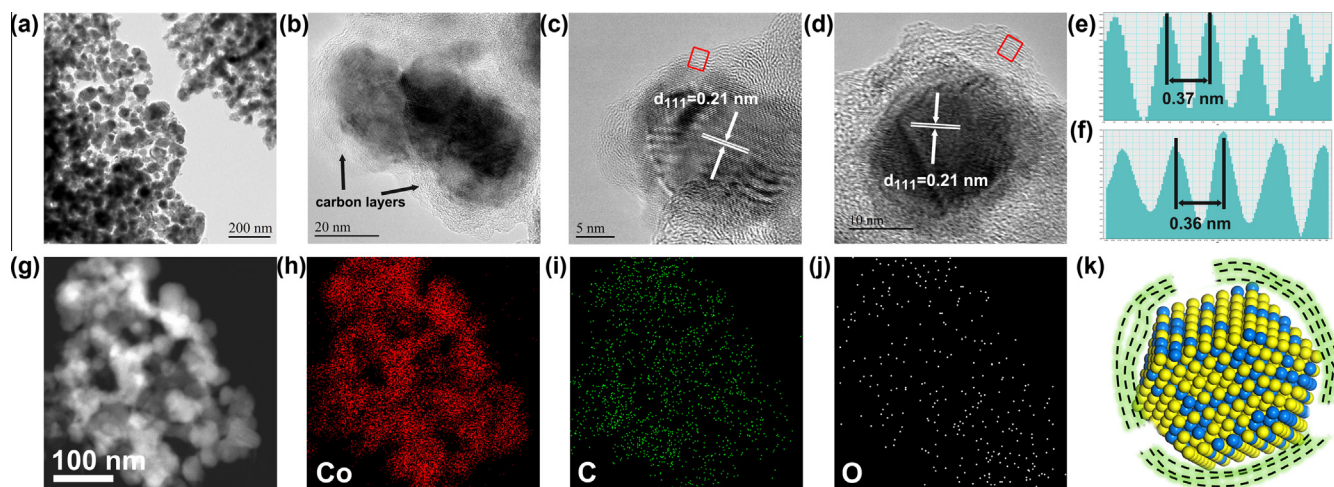


Fig. 1. Morphological characterizations of Co@C NPs. (a and b) Low-magnification TEM image of Co@C. The size of Co NPs ranges from ca. 20 to ca. 150 nm. Monodisperse Co NPs are separated by carbon layers, as shown in (b). (c and d) HRTEM images of Co NPs covered with carbon layers. (e and f) Profile of the carbon layers in selected areas in (c) and (d), respectively. The distance between two carbon layers is about 0.36–0.37 nm. (g) STEM-HAADF image of Co@C NPs. (h–j) Elemental mapping of Co, C, and O. (k) Schematic illustration of the structure of Co@C NPs. Blue balls stand for metallic Co and yellow balls stand for CoO_x . The surface of Co NP is mainly made up of CoO_x , while the core is metallic Co. The green circle surrounding the particle is the carbon layers with cracks. (For interpretation of the references to colour in this figure legend, the reader is referred to the web version of this article.)

mapping was performed and the results are displayed in Fig. 1g–j. They confirm that the Co NPs are covered by carbon layers. Meanwhile, oxygen can also be found in the sample, which may come from surface CoO_x and/or from the oxygenated groups in carbon layers. Contrast profiles of the carbon layers over Co NPs were also obtained, as presented in Fig. 1e and f. It can be seen there that the distance between the carbon layers is 0.34–0.37 nm, which corresponds to the distance between graphene layers. The thickness of most carbon layers is between 1 and 5 nm, with several layers of graphene [19]. A schematic illustration of the structure of Co@C NP is shown in Fig. 1k, indicating that the particle contains metallic Co as the core, some CoO_x patches on the surface, and carbon layers surrounding.

From the HRTEM images (Figs. S4–S6 in the Supporting Information), it can also be seen that the thin carbon layers over Co NPs are not closed, and some cracks can be found, implying that reactant molecules can have access to the Co NPs through the carbon layers. This can explain why the Co@C NPs could be partially oxidized by air under ambient conditions after the preparation procedure. In a recent work, Bao and his co-workers prepared a sample with CoNi alloy NPs totally encapsulated by several layers of graphene [20]. Those CoNi NPs were not soluble in a strong acid environment because of the protection of the carbon layers. However, in our case, Co NPs covered with cracked carbon layers can be almost totally dissolved in aqueous H_2SO_4 (photographs of the dissolving process can be seen in Fig. S7 in the Supporting Information), suggesting that Co@C NPs are not totally covered by carbon layers.

In general, due to the instability of metallic Co NPs, their preparation for heterogeneous catalytic application still remains a challenge. So far, metallic Co NPs have usually been prepared through a wet-chemistry method [21–23]. In these methods, Co NPs are capped with organic ligands to protect them from agglomeration and oxidation by air, but, at the same time, these long-chain organic ligands decrease the activity of Co NPs. Furthermore, Co NPs prepared by wet-chemistry methods are usually not stable under ambient conditions because of the oxidation of Co by air. In contrast, with the protection of carbon layers, the Co NPs prepared by our method can be stored under ambient conditions for over one month without obvious morphological changes. Only the oxidation of Co NPs at the surface occurs, and CoO_x patches

are formed that can easily be reduced by H_2 to metallic Co. Compared with previous reported pyrolysis methods (calcination at 800 °C), well-defined Co@C NPs with carbon layers can be directly synthesized at relatively lower temperatures. These air-stable Co@C NPs with CoO_x patches can be prepared on a large scale (several grams) in a facile way.

The bulk and surface properties of the Co@C NPs were also investigated. The XRD pattern of Co@C NPs is shown in Fig. 2a. Only the X-ray diffraction patterns of metallic Co can be observed with no X-ray diffraction peaks corresponding to other species, although the formation of CoO_x patches could be observed by HRTEM. The fact that CoO_x is not detected by XRD should be due to the small number of CoO_x patches in the Co@C sample. In the case of metallic Co, besides the cubic Co phase (PDF code 96-900-8467), a small amount of hexagonal Co phase (PDF code 96-900-8493) can also be observed in the XRD pattern. For metallic Co, the hexagonal close-packed (hcp) phase is more stable at lower temperature than the face-centered cubic (fcc) phase [24]. Since the Co-EDTA complex was decomposed and reduced at 450 °C, it is not surprising to see that both phases can exist [25].

The surface structures of Co@C NPs, as well as the carbon layers, were also studied by Raman spectroscopy. As indicated in Fig. 2b, vibration modes of Co_3O_4 (F_{2g} , E_g , and A_{1g}) can be observed [26]. Besides, the typical Raman signals of layered carbon, bands at 1318 cm^{-1} and 1595 cm^{-1} , can be observed, which corresponding to the D and G bands, respectively [27]. No peak related to the 2D band is detected between 2500 and 2800 cm^{-1} . The intensity ratio of the G band (I_G) to the D band (I_D) is ca. 0.8, suggesting that there is a large percentage of disorder in the structured carbon in Co@C NPs [28]. Combining these results and those from HRTEM images, it can be speculated that the degree of graphitization is relatively low in the carbon layers around Co NPs. Therefore, based on the structural characterizations, we can propose that Co@C NPs have core-shell structures with metallic Co as the core, CoO_x on the surface of Co crystallites, and thin layered carbon as the shell.

X-ray photoelectron spectroscopy (XPS) was employed to study the chemical state of Co in the as-prepared Co@C NPs. The Co@C NPs were reduced by H_2 at 7 bar and 120 °C (that condition will also be used in the hydrogenation reaction) within a prereactor integrated with the apparatus, and the sample is maintained isolated from any external contact during the entire process. The

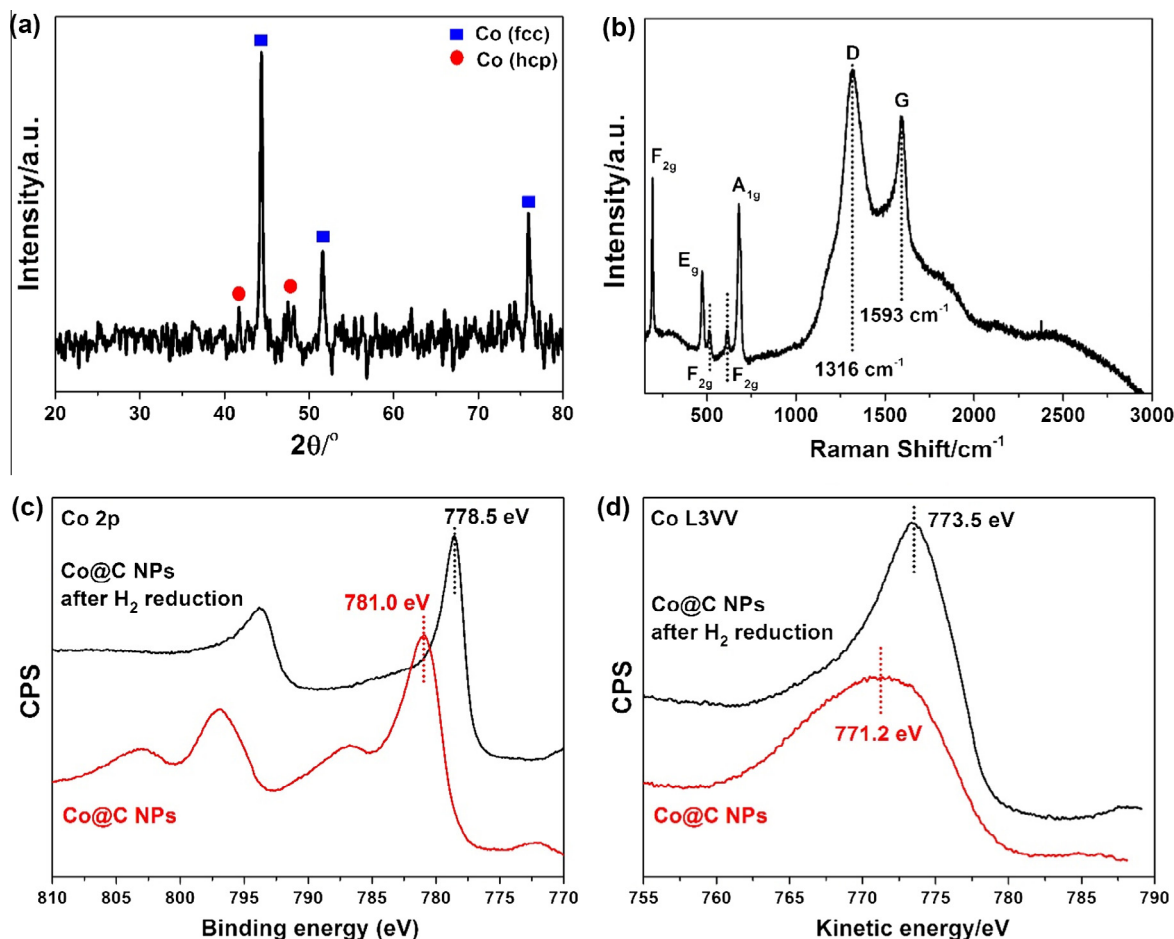


Fig. 2. Structural characterizations of Co@C NPs. (a) XRD pattern of fresh Co@C NPs, (b) Raman spectrum of Co@C NPs, (c) XPS spectra of Co2p region, and (d) Co L3VV Auger spectra of the fresh Co@C NPs and the sample after ex situ reduction by 7 bar of H₂ at 120 °C.

XPS spectra of the Co2p region and the Auger spectra of Co L3VV are shown in Fig. 2c and d, respectively. In the as-prepared Co@C sample, only CoO_x can be observed, which can be ascribed to the CoO_x patches on the surfaces of Co NPs [29]. After H₂ reduction treatment (7 bar of H₂ at 120 °C), the CoO_x is totally transformed into metallic Co, as confirmed by both Co2p XPS and Co L3VV Auger spectra. In the fresh as-prepared catalyst, N is presented in the sample, as shown by elemental mapping (see Fig. S8 in the Supporting Information). However, after the ex situ reduction treatment, no N can be found in the sample by XPS, indicating that there are practically no N species in the working catalyst.

With the characterization results presented up to now, we can say that during preparation of Co@C NPs, Co NPs of 20–150 nm were generated, which have a metallic Co core with CoO_x on the surface, surrounded by disordered carbon layers. Moreover, under reduction conditions, which are the same that are used for performing the catalytic test, the CoO_x patches can be totally reduced to metallic Co.

3.2. Catalytic results

At this point, the chemoselective hydrogenation of 3-nitrostyrene was chosen as a model reaction to study the catalytic properties of Co@C NPs and to see if the non-noble metal cobalt nanoparticles can behave as a chemoselective catalyst. To test this, the same reaction conditions that showed chemoselective hydrogenation when noble metal catalysts were used, i.e., 120 °C and 7 bar of H₂, were selected [4,5]. Notice that these are much milder

conditions than those reported for the hydrogenation of 3-nitrostyrene with Co- and Fe-based catalysts [10,11]. The reaction conditions and catalytic results are given in Fig. 3. It can be seen there that fresh Co@C NPs are active and selective catalyst for the hydrogenation of 3-nitrostyrene. When the conversion of 3-nitrostyrene is 95%, the selectivity to 3-aminostyrene is 93%, which is comparable to the values obtained with noble metal catalysts [4,5]. The initial TOF calculated based on surface Co atoms is ca. 8.2 h⁻¹ according to the particle size distribution of Co@C NPs. Notably, a reaction induction period of about 20–30 min can be observed in the kinetic curve (Fig. S9 in the Supporting Information) starting with the fresh catalyst that contains a core of metallic cobalt and a shell of CoO_x. In accord with XPS results, this induction period could be caused by the time required for the reduction of surface CoO_x to metallic Co under the reaction conditions. As presented in Fig. S10 in the Supporting Information, the morphology and particle size distribution after reduction under reaction conditions are similar to those for the fresh Co@C sample, suggesting that no structural changes or agglomeration have occurred. HRTEM images of the used sample also confirm that metallic Co NPs are still surrounded by carbon layers. Therefore, the above morphological characterization indicates that the nanoscale structures of the Co@C NPs sample are stable under reaction conditions.

In a recent work, Zhang et al. have demonstrated that atomically dispersed Co species in the carbon matrix can serve as the active sites for oxidation reactions [30]. Here, in order to exclude the role of atomically dispersed Co species in the hydrogenation reaction, we have also measured the residual solid after the acid

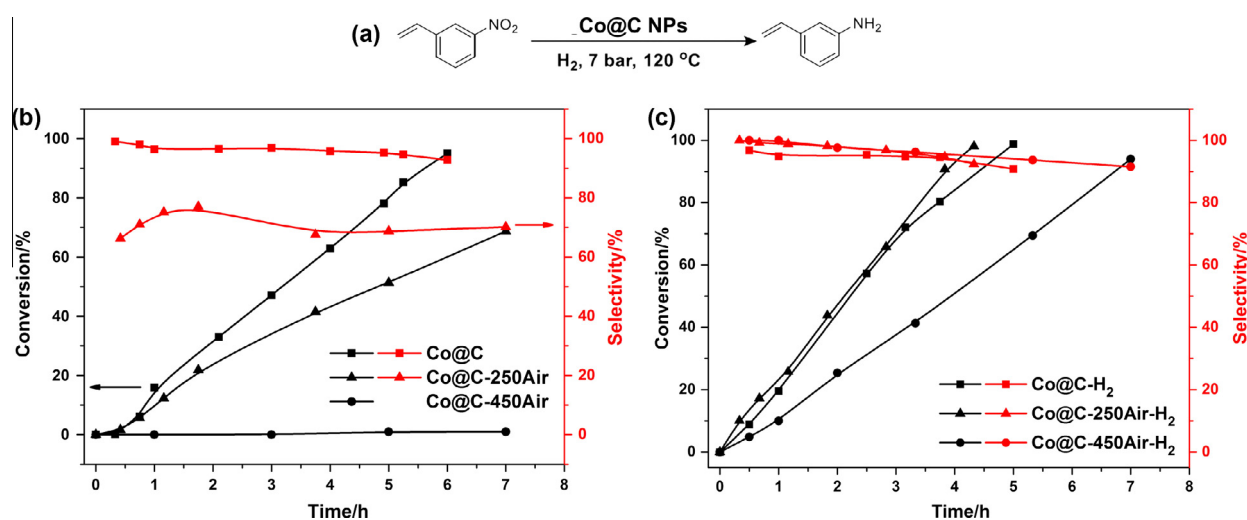


Fig. 3. (a) Reaction scheme of the chemoselective hydrogenation of 3-nitrostyrene. Reaction conditions: 0.5 mmol 3-nitrostyrene, 30 mg Co@C NPs as catalyst, 2 mL toluene as solvent, 30 μ L dodecane as internal standard. (b) Catalytic performance of Co@C, Co@C-250Air, and Co@C-450Air in chemoselective hydrogenation of 3-nitrostyrene to 3-aminostyrene. The black and red legends correspond to conversion and selectivity, respectively. (c) Catalytic performance of Co@C-H₂, Co@C-250Air-H₂, and Co@C-450Air-H₂ in chemoselective hydrogenation of 3-nitrostyrene to 3-aminostyrene. The black and red legends correspond to conversion and selectivity, respectively. (For interpretation of the references to colour in this figure legend, the reader is referred to the web version of this article.)

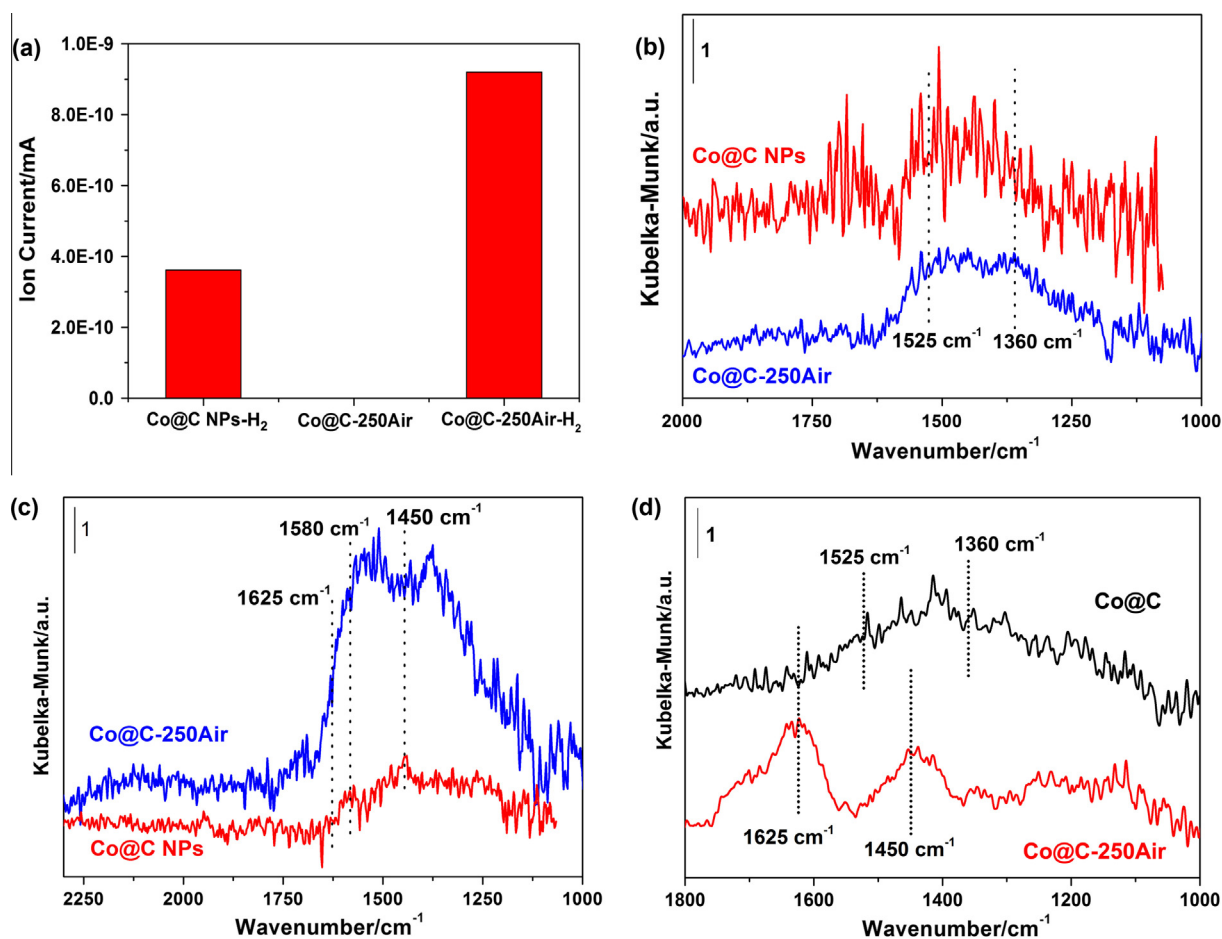


Fig. 4. H₂-D₂ exchange and DRIFTS adsorption experiments. (a) Enhancement of the ion current in the mass signal of HD during the H₂-D₂ exchange experiment over Co@C-H₂, Co@C-250Air, and Co@C-250Air-H₂ NPs at 80 °C. (b) DRIFTS of adsorbed nitrobenzene, (c) DRIFTS of adsorbed styrene, and (d) DRIFTS of co-adsorbed nitrobenzene and styrene on Co@C NPs and Co@C-250Air sample.

leaching treatment (as shown in Fig. S7 in the Supporting Information). No activity can be observed in the hydrogenation of 3-nitrostyrene, suggesting that the metallic Co NPs should be the active sites for hydrogenation reactions.

The recyclability of Co@C NPs in the hydrogenation of 3-nitrostyrene was also tested. Since metallic Co NPs are paramagnetic, the separation of the solid catalyst from the liquid was very facile with the help of a magnetic bar [31,32] (see Fig. S11 in the

Supporting Information). After being washed several times with toluene, the catalyst can be reused without further treatment, and the Co@C catalyst shows good activity and selectivity for five recycles (see Table S1 in the Supporting Information).

3.3. Role of the carbon layers in the catalyst

At this point, we know that the reduced Co@C NPs are active and chemoselective for reduction of substituted nitroarenes into corresponding anilines under mild reaction conditions. To investigate if the carbon layers play an intrinsic role in the chemoselective hydrogenation reaction, calcination of the Co@C NPs at 250 and 450 °C in air was performed to remove the carbon layers on the nanoparticles. The samples after calcination in air are denoted as Co@C-250Air and Co@C-450Air, respectively. From the Raman spectra (Fig. S12 in the Supporting Information), we find that in Co@C-250Air, bands at 1318 and 1595 cm^{-1} are still visible, indicating that part of the carbon layers is still preserved. In Co@C-450Air, the above Raman bands are already very weak, suggesting that almost all the carbon layers have already been removed. As shown in Fig. 3b, it is possible to see that activity and selectivity drop when Co@C-250Air is used, while Co@C-450Air shows no activity in the hydrogenation reaction. The product distribution in the hydrogenation of 3-nitrostyrene with a Co@C-250Air sample as the catalyst is shown in Fig. S13. To explain these changes, TEM is used to clarify the structural transformation occurring with Co@C NPs after calcination in air. As shown in Fig. S14, metallic Co NPs crack into smaller CoO_x NPs after calcination in air at 250 °C, which has also been observed in other works [33]. The crystal lattice fringes of CoO_x NPs can be observed in the HRTEM images, though there are still some particles with metallic Co phase in the Co@C-250Air sample. Some carbon layers can still be found on Co- CoO_x and CoO_x NPs in Co@C-250Air, as confirmed by Raman spectra. It should be noted that part of the carbon layers were burned during the calcination in air, resulting in the formation of naked Co and CoO_x NPs.

In the Co@C-450Air sample (shown in Fig. S15 in the Supporting Information), Co NPs are totally converted into Co_3O_4 NPs. The phase composition of the samples after calcination in air can also be measured by selective area electron diffraction (SAED). As can be seen in Fig. S16, metallic Co NPs transform into a mixture of Co and Co_3O_4 when calcined at 250 °C, and to pure Co_3O_4 when calcined at 450 °C. Considering the significant decrease of activity observed when the Co@C sample was calcined at 250 °C and even more when the temperature was 450 °C, it can be deduced that CoO_x or Co_3O_4 cannot be the catalytically active phase.

Co@C, Co@C-250Air, and Co@C-450Air NPs were reduced in the batch reactor under higher temperature and H_2 pressure (200 °C, 10 bar H_2) before the hydrogenation reaction to reduce the CoO_x species to metallic Co. After the reduction pretreatment, 3-nitrostyrene was added and the hydrogenation reaction was performed at 7 bar of H_2 and 120 °C. As presented in Fig. 3c, Co@C- H_2 gives a kinetic curve similar to that for pristine Co@C, except for the disappearance of the induction period due to the reduction pretreatment. However, the situation changes a lot in the case of Co@C-250Air and Co@C-450Air. The Co@C-250Air- H_2 sample shows higher activity than pristine Co@C NPs and very good selectivity. This would indicate that the metallic Co NPs formed after reduction of Co@C-250Air should be responsible for the high activity and selectivity in hydrogenation reaction observed with Co@C-250Air- H_2 . What is more, the reduction pretreatment also has a significant effect on Co@C-450Air. After H_2 reduction, the Co@C-450Air- H_2 sample shows moderate activity and high selectivity, which further indicates that the chemoselective hydrogenation of 3-nitrostyrene is related to metallic Co and the role of

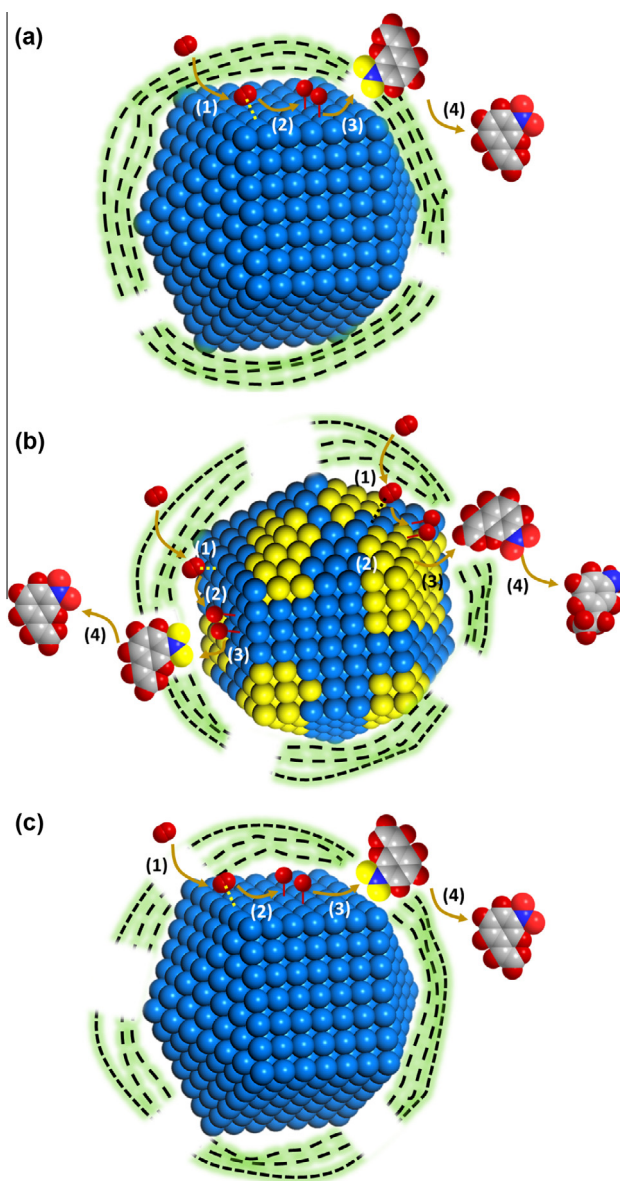


Fig. 5. Proposed reaction pathways of hydrogenation of 3-nitrostyrene on Co@C NPs with coverage of carbon layers (a) and defective coverage of carbon layers (b). In schematic illustration (a), the chemoselective hydrogenation of $-\text{NO}_2$ groups can be divided into the following steps: the diffusion of H_2 from the gas phase up to the surface of metallic Co NPs (1), activation of H_2 (2), adsorption of the nitro aromatic (3), and H-transfer from Co NPs to $-\text{NO}_2$ groups (4) for selective hydrogenation of $-\text{NO}_2$ groups. In the scheme presented in (b), a sample with Co_3O_4 patches after removal of part of the carbon layers, hydrogenation of $-\text{NO}_2$ and $\text{C}=\text{C}$ groups can be divided into following steps: diffusion of H_2 to the surface of metallic Co NPs (1), activation of H_2 (2), hydrogen transfer (3), and hydrogenation of both $-\text{NO}_2$ and $\text{C}=\text{C}$ groups (4). In schematic illustration (c), for the in situ reduced sample after removal of part of carbon layers, the chemoselective hydrogenation of $-\text{NO}_2$ groups can be divided into several steps, including the diffusion of H_2 to the surface of metallic Co NPs (1), activation of H_2 (2), H-transfer from Co NPs to $-\text{NO}_2$ groups (3), and selective hydrogenation of $-\text{NO}_2$ groups (4).

carbon layers in Co@C NPs is mainly to protect Co NPs from overoxidation by air.

3.4. In situ adsorption spectroscopy

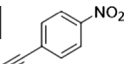
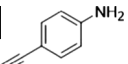
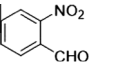
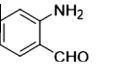
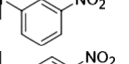
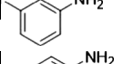
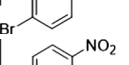
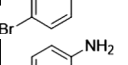
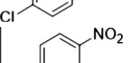
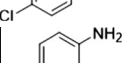
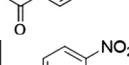
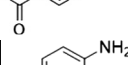
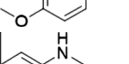
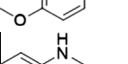
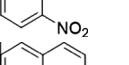
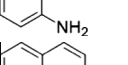
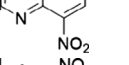
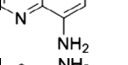
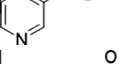
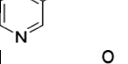
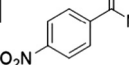
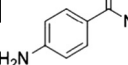
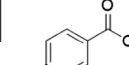
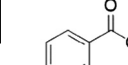
In order to explain the activity and high selectivity of Co@C NPs, H_2 - D_2 exchange and the adsorption of substrates on Co@C NPs followed by diffuse reflectance infrared Fourier transform

spectroscopy (DRIFTS) were carried out. The H₂–D₂ exchange rates on Co NPs and Co@C–250Air (with and without H₂ prereduction) are shown in Fig. 4a. H₂–D₂ exchange can be observed on Co@C NPs. Interestingly, as displayed in Fig. S17 in the Supporting Information, a large amount of H₂ was released from Co NPs when the atmosphere was changed from H₂ to Ar after the in situ reduction process. The H₂ released should come from the H₂ adsorbed by Co NPs [34,35]. It appears then that H₂ diffuses through the potential cracks present in carbon layers and is activated on the surface of Co NPs. In the case of Co@C–250Air, no H₂–D₂ exchange can be observed when the sample is not prereduced. After H₂ pretreatment, the H₂–D₂ exchange rate is higher on Co@C–250Air–H₂ than on Co@C, suggesting that more Co sites are exposed after the removal of carbon layers and the reduction of CoO_x. The H₂–D₂ exchange experiments further confirm that metallic Co are the active sites for H₂ activation and carbon layers are not playing a direct role in the catalytic process.

We have found in previous work that the way that the reactant is adsorbed on metal catalysts can determine the chemoselectivity during hydrogenation of substituted nitroaromatics [36]. Thus, in order to explain different catalytic behavior of Co@C NPs and Co@C–250Air samples for chemoselective hydrogenation of 3-nitrostyrene, we have performed in situ IR adsorption experiments by DRIFTS, with nitrobenzene and styrene as probe molecules. For comparison, the IR spectra of nitrobenzene and styrene on KBr

substrate have also been measured (see Fig. S18 in the Supporting Information). The adsorption spectra of the probe molecules on Co@C and Co@C–250Air are shown in Fig. S19. The IR adsorption spectra of nitrobenzene on Co@C and Co@C–250Air samples show wide IR bands between 1600 and 1250 cm^{−1} in both samples (see Fig. 4b). The vibration bands of –NO₂ groups can be observed at ca. 1525 and 1360 cm^{−1} [37,38]. The intensity of the IR bands is similar on both samples, suggesting that the adsorption spectra of Co@C and Co@C–250Air for nitrobenzene are similar. On the other hand, the adsorption spectra of styrene on Co@C and Co@C–250Air (Fig. 4c) are significantly different. Indeed, as can be seen in Fig. 4c, the IR band corresponding to the aromatic ring can be observed between 1580 and 1450 cm^{−1}, with the vibration mode of the C=C bond at ca. 1625 cm^{−1} [39]. Co@C–250Air shows much stronger adsorption of styrene than the Co@C sample, indicating that the adsorption of styrene onto CoO_x NPs will be enhanced when metallic Co NPs are oxidized. We have also studied the co-adsorption of nitrobenzene and styrene on Co@C and Co@C–250Air by DRIFTS. As can be seen in Fig. 4d, only the adsorption of nitrobenzene can be observed on Co@C, while strong adsorption of styrene occurs on Co@C–250Air. In the case of Co@C–450Air, only the adsorption of styrene can be observed after the evacuation (see Fig. S20 in the Supporting Information). Therefore, based on the IR adsorption results, we can conclude that the chemical states of Co have a significant influence on the adsorption properties of substrate

Table 1
Scope of the hydrogenation of nitroarenes catalyzed by Co@C NPs.

Entry	Substrate	Product	Time (h)	H ₂ pressure (bar)	Temp. (°C)	Con. (%)	Sel. (%)
1			6	7	120	93	95
2 [†]			12	10	100	95	95
3			5	10	140	99	97
4			10	10	140	95	99
5			8	10	140	99	97
6			12	10	140	99	95
7			10	8	120	99	99
8			10	8	120	91	93
9			15	10	140	98	95
10			15	10	140	99	95
11 [‡]			10	10	140	97	99
12			10	10	140	97	99

Notes: Reaction conditions: Co@C NPs is 30 mg, 0.5 mmol nitroarenes, 30 μ L dodecane as the internal standard, 2 mL toluene as the solvent.

[†] 100 mg Co@C NPs as the catalyst.

[‡] 2 mL THF as the solvent.

molecules in Co@C NPs. For metallic Co NPs, only $-\text{NO}_2$ groups will be preferentially adsorbed. In contrast, when the Co NPs are partially oxidized, the $\text{C}=\text{C}$ instead of $-\text{NO}_2$ groups will be preferentially adsorbed. The selective adsorption observed in above experiments can explain the differences for the chemoselective hydrogenation of 3-nitrostyrene on metallic and partially oxidized cobalt nanoparticles.

3.5. Catalytic mechanism

It appears then that unless Co nanoparticles are reduced to metallic nanoparticles, their activity and selectivity will be relatively low. In the case where partial (surface) oxidation occurs, not only is the hydrogenation activity low, but also it will favor adsorption of styrene versus nitrobenzene, which can further favor the loss of chemoselectivity during the hydrogenation of 3-nitrostyrene.

Based on the above catalytic results and spectroscopic characterizations, we propose a reaction mechanism of chemoselective hydrogenation of 3-nitrostyrene on Co@C NPs covered with disordered carbon layers. Three cases with different oxidation states of Co and coverages of carbon layers are considered. As shown in Fig. 5, the first step in the hydrogenation reaction catalyzed by both Co@C and Co@C-250Air is the diffusion of H_2 to the surface of Co NPs under the cover of carbon layers. Then H_2 will be activated by Co NPs and form active H species. The third step will be different for Co@C and Co@C-250Air due to their different adsorption properties to the substrate molecules. In the case of Co@C (Fig. 5a), 3-nitrostyrene will be adsorbed onto metallic Co preferentially through the $-\text{NO}_2$ groups, which will be reduced by the active H species formed on Co NPs. The adsorption of $\text{C}=\text{C}$ bond on the Co@C sample is relatively weak. However, in the case of Co@C-250Air (Fig. 5b), both $\text{C}=\text{C}$ and $-\text{NO}_2$ groups can have direct access to the surface of Co NPs. As a consequence, both $-\text{NO}_2$ and $\text{C}=\text{C}$ groups can be hydrogenated by H_2 , resulting in lower selectivity. When Co@C-250Air is reduced by H_2 before the catalytic test (Fig. 5c), more metallic Co sites will selectively absorb $-\text{NO}_2$ groups instead of $\text{C}=\text{C}$ bonds, leading to high activity and selectivity.

3.6. Scope of the catalyst

The scope of Co@C NPs in hydrogenation of substituted nitroarenes was investigated by reacting substituted nitrobenzene with halogens, amides, and ester groups. In all cases, activity and chemoselectivity were high under mild reaction conditions (Table 1). Selective hydrogenation of $-\text{NO}_2$ groups can be performed in the presence of groups such as olefins, alkynes, and carbonyls under much lower H_2 pressure (7–10 bar) than in previous reports (30–50 bar) [10–12]. As can be seen in Table 1, all the substrates can be selectively transformed with over 93% selectivity. Most of the entries show over 90% yield for both electron-deficient and electron-rich substituents. Co@C NPs are also active and selective for nitroarenes, with easily reducible moieties including alkynes, ketones, and halogens. In previous work, the yields of heteroaromatic amines were not very high (from 53% to 75%). With Co@C NPs, we can get much higher yields of heteroaromatic amines (Entries 9 and 10 in Table 1). Thus, Co@C NPs are superior catalysts for chemoselective hydrogenation of nitroarenes under mild conditions.

4. Conclusions

In this work, we present a strategy for the synthesis of Co@C NPs. Metallic Co NPs are covered with thin carbon layers with

small cracks. H_2 can diffuse through the cracks in the thin carbon layers and be activated at room temperature. The existence of carbon layers can protect the Co NPs from overoxidation by air. This type of material shows good activity and selectivity for hydrogenation of nitroarenes, with wide scope and good tolerance. It can also give high yields of heteroaromatic amines. The adsorption properties of substrate molecules will be affected by the chemical state of Co. Combining with in situ IR adsorption experiments and results from electron microscopy, a reaction mechanism is proposed in which the important role of metallic cobalt and the negative role of CoO_x in the selective hydrogenation reaction is shown. Nondirect involvement of the carbon in the reaction is also proposed. The role of carbon layers is as protection of the Co NPs from getting deeply oxidized. This work provides new insight into design of non-noble metal catalysts for heterogeneous catalytic applications.

Acknowledgments

L.L. thanks ITQ for a contract. The European Union is also acknowledged by ERC-AdG-2014-671093-SynCatMatch. The authors also thank the Microscopy Service of UVP for kind help with TEM and STEM measurements.

Appendix A. Supplementary material

Supplementary data associated with this article can be found, in the online version, at <http://dx.doi.org/10.1016/j.jcat.2016.04.006>.

References

- [1] H.-U. Blaser, U. Siegrist, H. Steiner (Eds.), *Aromatic Nitro Compounds: Fine Chemicals Through Heterogeneous Catalysis*, Wiley-VCH, Weinheim, Germany, 2001.
- [2] A. Corma, P. Serna, Chemoselective hydrogenation of nitro compounds with supported gold catalysts, *Science* 313 (2006) 332–334.
- [3] H.-U. Blaser, H. Steiner, M. Studer, Selective catalytic hydrogenation of functionalized nitroarenes: an update, *ChemCatChem* 1 (2009) 210–221.
- [4] A. Corma, P. Serna, P. Concepcion, J.J. Calvino, Transforming nonselective into chemoselective metal catalysts for the hydrogenation of substituted nitroaromatics, *J. Am. Chem. Soc.* 130 (2008) 8748–8753.
- [5] P. Serna, M. Boronat, A. Corma, Tuning the behavior of Au and Pt catalysts for the chemoselective hydrogenation of nitroaromatic compounds, *Top. Catal.* 54 (2011) 439–446.
- [6] J. Ran, J. Zhang, J. Yu, M. Jaroniec, S.Z. Qiao, Earth-abundant cocatalysts for semiconductor-based photocatalytic water splitting, *Chem. Soc. Rev.* 43 (2014) 7787–7812.
- [7] H.R. Byon, J. Suntivich, Y. Shao-Horn, Graphene-based non-noble-metal catalysts for oxygen reduction reaction in acid, *Chem. Mater.* 23 (2011) 3421–3428.
- [8] R.V. Jagadeesh, H. Junge, M. Beller, Green synthesis of nitriles using non-noble metal oxides-based nanocatalysts, *Nat. Commun.* 5 (2014) 4123.
- [9] B. Su, Z.C. Cao, Z.J. Shi, Exploration of earth-abundant transition metals (Fe, Co, and Ni) as catalysts in unreactive chemical bond activations, *Acc. Chem. Res.* 48 (2015) 886–896.
- [10] F.A. Westerhaus, R.V. Jagadeesh, G. Wienhofer, M.M. Pohl, J. Radnik, A.E. Surkus, J. Rabeah, K. Junge, H. Junge, M. Nielsen, A. Bruckner, M. Beller, Heterogenized cobalt oxide catalysts for nitroarene reduction by pyrolysis of molecularly defined complexes, *Nat. Chem.* 5 (2013) 537–543.
- [11] R.V. Jagadeesh, A.E. Surkus, H. Junge, M.M. Pohl, J. Radnik, J. Rabeah, H. Huan, V. Schunemann, A. Bruckner, M. Beller, Nanoscale Fe_2O_3 -based catalysts for selective hydrogenation of nitroarenes to anilines, *Science* 342 (2013) 1073–1076.
- [12] Z. Wei, J. Wang, S. Mao, D. Su, H. Jin, Y. Wang, F. Xu, H. Li, Y. Wang, In situ-generated $\text{Co}^0\text{-Co}_3\text{O}_4/\text{N-doped carbon nanotubes}$ hybrids as efficient and chemoselective catalysts for hydrogenation of nitroarenes, *ACS Catal.* 5 (2015) 4783–4789.
- [13] T. Fu, M. Wang, W. Cai, Y. Cui, F. Gao, L. Peng, W. Chen, W. Ding, Acid-resistant catalysis without use of noble metals: carbon nitride with underlying nickel, *ACS Catal.* 4 (2014) 2536–2543.
- [14] V. Berry, Impermeability of graphene and its applications, *Carbon* 62 (2013) 1–10.
- [15] J.S. Bunch, S.S. Verbridge, J.S. Alden, A.M. van der Zande, J.M. Parpia, H.G. Craighead, P.L. McEuen, Impermeable atomic membranes from graphene sheets, *Nano Lett.* 8 (2008) 2458–2462.
- [16] N. Fairley, CasaXPS Version 2.3.14, Casa Software Ltd., 2008.

- [17] W. Zhong, H. Liu, C. Bai, S. Liao, Y. Li, Base-free oxidation of alcohols to esters at room temperature and atmospheric conditions using nanoscale co-based catalysts, *ACS Catal.* 5 (2015) 1850–1856.
- [18] M.R. Ward, E.D. Boyes, P.L. Gai, In situ aberration-corrected environmental TEM: reduction of model Co_3O_4 in H_2 at the atomic level, *ChemCatChem* 5 (2013) 2655–2661.
- [19] L. Qiu, J.Z. Liu, S.L. Chang, Y. Wu, D. Li, Biomimetic superelastic graphene-based cellular monoliths, *Nat. Commun.* 3 (2012) 1241.
- [20] J. Deng, P. Ren, D. Deng, X. Bao, Enhanced electron penetration through an ultrathin graphene layer for highly efficient catalysis of the hydrogen evolution reaction, *Angew. Chem. Int. Ed.* 54 (2015) 2100–2104.
- [21] S. Sun, C.B. Murray, Synthesis of monodisperse cobalt nanocrystals and their assembly into magnetic superlattices, *J. Appl. Phys.* 85 (1999) 4325.
- [22] S. Guo, S. Zhang, L. Wu, S. Sun, Co/CoO nanoparticles assembled on graphene for electrochemical reduction of oxygen, *Angew. Chem. Int. Ed.* 51 (2012) 11770–11773.
- [23] Y. Lu, X. Lu, B.T. Mayers, T. Herricks, Y. Xia, Synthesis and characterization of magnetic Co nanoparticles: a comparison study of three different capping surfactants, *J. Solid State Chem.* 181 (2008) 1530–1538.
- [24] X.Q. Zhao, S. Veintemillas-Verdaguer, O. Bomati-Miguel, M.P. Morales, H.B. Xu, Thermal history dependence of the crystal structure of Co fine particles, *Phys. Rev. B* 71 (2005).
- [25] V.C.A. de la Peña O'Shea, P.R.R. de la Piscina, N. Homs, G. Aromí, J.L.G. Fierro, Development of hexagonal closed-packed cobalt nanoparticles stable at high temperature, *Chem. Mater.* 21 (2009) 5637–5643.
- [26] V.G. Hadjiev, M.N. Iliev, I.V. Vergilov, The Raman spectra of Co_3O_4 , *J. Phys. C Solid State Phys.* 21 (1988) L199–L201.
- [27] A.C. Ferrari, J. Robertson, Raman spectroscopy of amorphous, nanostructured, diamond-like carbon, and nanodiamond, *Phil. Trans. R. Soc. A* 362 (2004) 2477–2512.
- [28] Y. Wang, D.C. Alsmeyer, R.L. McCreery, Raman spectroscopy of carbon materials: structural basis of observed spectra, *Chem. Mater.* 2 (1990) 557–563.
- [29] V. Iablokov, S.K. Beaumont, S. Alayoglu, V.V. Pushkarev, C. Specht, J. Gao, A.P. Alivisatos, N. Kruse, G.A. Somorjai, Size-controlled model Co nanoparticle catalysts for CO_2 hydrogenation: synthesis, characterization, and catalytic reactions, *Nano Lett.* 12 (2012) 3091–3096.
- [30] L. Zhang, A. Wang, W. Wang, Y. Huang, X. Liu, S. Miao, J. Liu, T. Zhang, Co–N–C catalyst for C–C coupling reactions: on the catalytic performance and active sites, *ACS Catal.* 5 (2015) 6563–6572.
- [31] D. Wang, D. Astruc, Fast-growing field of magnetically recyclable nanocatalysts, *Chem. Rev.* 114 (2014) 6949–6985.
- [32] M.B. Gawande, P.S. Branco, R.S. Varma, Nano-magnetite (Fe_3O_4) as a support for recyclable catalysts in the development of sustainable methodologies, *Chem. Soc. Rev.* 42 (2013) 3371–3393.
- [33] H. Wang, C. Chen, Y. Zhang, L. Peng, S. Ma, T. Yang, H. Guo, Z. Zhang, D.S. Su, J. Zhang, In situ oxidation of carbon-covered cobalt nanocapsules creates highly active cobalt oxide catalysts for hydrocarbon combustion, *Nat. Commun.* 6 (2015) 7181.
- [34] C.H. Bartholomew, R.C. Reuel, Cobalt-support interactions: their effects on adsorption and carbon monoxide hydrogenation activity and selectivity properties, *Ind. Eng. Chem. Prod. Res. Dev.* 24 (1985) 56–61.
- [35] I.C. Yates, C.N. Satterfield, Intrinsic kinetics of the Fischer–Tropsch synthesis on a cobalt catalyst, *Energy Fuels* 5 (1991) 168–173.
- [36] M. Boronat, P. Concepcion, A. Corma, S. Gonzalez, F. Illas, P. Serna, A molecular mechanism for the chemoselective hydrogenation of substituted nitroaromatics with nanoparticles of gold on TiO_2 catalysts: a cooperative effect between gold and the support, *J. Am. Chem. Soc.* 129 (2007) 16230–16237.
- [37] I. Ahmad, T.J. Dines, C.H. Rochester, J.A. Anderson, IR study of nitrotoluene adsorption on oxide surfaces, *Faraday Trans.* 92 (1996) 3225.
- [38] C.A. Koutstaal, P.A.J.M. Angevaere, E.J. Grootendorst, V. Poncet, On the adsorption and surface reactions of nitro- and nitrosobenzene on oxides: an IR study, *J. Catal.* 141 (1993) 82–93.
- [39] B. Bachiller-Baeza, J.A. Anderson, FTIR and reaction studies of styrene and toluene over silica–zirconia-supported heteropoly acid catalysts, *J. Catal.* 212 (2002) 231–239.